Atomic-layer-resolved composition and electronic structure of the cuprate $Bi_2Sr_2CaCu_2O_{8+\delta}$ from soft x-ray standing-wave photoemission

Cheng-Tai Kuo,[1,2,*] Shih-Chieh Lin,[1,2] Giuseppina Conti,[1,2] Shu-Ting Pi,[1] Luca Moreschini,[3] Aaron Bostwick,[3] Julia Meyer-Ilse,[2] Eric Gullikson,[2] Jeffrey B. Kortright,[2] Slavomír Nemšák,[3,4] Julien E. Rault,[5] Patrick Le Fèvre,[5] François Bertran,[5] Andrés F. Santander-Syro,[6] Ivan A. Vartanyants,[7,8] Warren E. Pickett,[1] Romuald Saint-Martin,[9] Amina Taleb-Ibrahimi,[10] and Charles S. Fadley[1,2,†]

[1]*Department of Physics, University of California Davis, Davis, California 95616, USA*
[2]*Materials Sciences Division, Lawrence Berkeley National Laboratory, Berkeley, California 94720, USA*
[3]*Advanced Light Source, Lawrence Berkeley National Laboratory, Berkeley, California 94720, USA*
[4]*Peter Grünberg Institut PGI-6, Research Center Jülich, 52425 Jülich, Germany*
[5]*Synchrotron SOLEIL, L'Orme des Merisiers, Saint-Aubin-BP48, 91192 Gif-sur-Yvette, France*
[6]*CSNSM, Université Paris-Sud, CNRS/IN2P3, Université Paris-Saclay, 91405 Orsay Cedex, France*
[7]*Deutsches Elektronen-Synchrotron DESY, Notkestraße 85, D-22607 Hamburg, Germany*
[8]*National Research Nuclear University MEPhI (Moscow Engineering Physics Institute), Kashirskoe Shosse 31, Moscow 115409, Russia*
[9]*SP2M-ICMMO-UMR-CNRS 8182, Université Paris-Sud, Université Paris-Saclay, 91405 Orsay Cedex, France*
[10]*UR1 CNRS/Synchrotron SOLEIL, Saint-Aubin, 91192 Gif sur Yvette, France*

(Received 6 July 2018; published 19 October 2018)

A major remaining challenge in the superconducting cuprates is the unambiguous differentiation of the composition and electronic structure of the CuO_2 layers and those of the intermediate layers. The large c axis for these materials permits employing soft x-ray (930.3 eV) standing wave (SW) excitation in photoemission that yields atomic layer-by-layer depth resolution of these properties. Applying SW photoemission to $Bi_2Sr_2CaCu_2O_{8+\delta}$ yields the depth distribution of atomic composition and the layer-resolved densities of states. We detect significant Ca presence in the SrO layers and oxygen bonding to three different cations. The layer-resolved valence electronic structure is found to be strongly influenced by the atomic supermodulation structure, as determined by comparison to density functional theory calculations, by Ca-Sr intermixing, and by correlation effects associated with the Cu 3*d*-3*d* Coulomb interaction, further clarifying the complex interactions in this prototypical cuprate. Measurements of this type for other quasi-two-dimensional materials with large c represent a promising future direction.

DOI: 10.1103/PhysRevB.98.155133

I. INTRODUCTION

The cuprate high-temperature superconductors have attracted much attention and have been extensively studied, but are still not fully understood. It is believed that superconductivity is related to hole- or electron- doping within their layered quasi-two-dimensional (2D) crystallographic structures, with the key element being the CuO_2 planes [1,2]. Characterizing this basic element in superconductivity is thus critical, and some important challenges remaining are to differentiate the electronic structure of the CuO_2 layers from those of the intermediate layers, as well as the elemental composition of each layer.

Photoemission spectroscopy, especially angle-resolved photoemission spectroscopy (ARPES), is one of the most powerful techniques for visualizing the electronic structure in materials [1,3,4]. Conventional ARPES measurements are performed with excitation energies of ∼20–150 eV that yield high surface sensitivity due to the short electron inelastic mean-free paths (IMFP, λ_{IMFP}) [5] of ∼3–6 Å. For materials with small unit-cell dimensions perpendicular to the surface and inert, easily cleavable or *in situ* preparable surfaces, ARPES can provide unique information on properties close to that of bulk. However, for materials with large c-axis parameters, e.g., the cuprates, it can be argued that conventional ARPES preferentially samples the topmost atomic layers rather than the full unit cell. For example, in the case of $Bi_2Sr_2CaCu_2O_{8+\delta}$ (Bi2212), the c-axis parameter is ∼30.7 Å, and its first CuO_2 layer in the unit cell is ∼6 Å below the cleaved surface; thus, for conventional ARPES, the contributions from the first CuO_2 layer will be attenuated by $\sim e^{-1} = 0.37$, and they will be even more extreme for the deeper layers. Beyond this, in conventional ARPES, the only way to distinguish element-specific behavior is to use resonant photoemission that would selectively enhance the different layer contributions [6,7]. But quantitative interpretation of resonant photoemission is difficult, and the number of elements that can be studied is limited by the suitable core levels to excite resonantly. Standing-wave (SW) photoemission provides a method to get around these limitations of conventional ARPES and resonant photoemission.

X-ray SW excitation with energy ∼2–10 keV in connection with spectroscopy was introduced some time ago [8], and its theory and applications have been reviewed in detail [9]. SW

*Corresponding author: chengtaikuo@lbl.gov
†Corresponding author: fadley@lbl.gov

 ©2018 American Physical Society

hard x-ray photoemission at a few keV has been used to derive the spatial distribution of composition and differentiate the element-specific matrix-element weighted densities of states (DOSs) within the unit cells of several solids [10–12], including $YBa_2Cu_3O_{7-\delta}$ (YBCO) [13]. For higher photon energies above the ∼1 keV regime, these DOSs can be considered to be weighted by differential atomic cross sections, and it is at this level that we will analyze our data.

In this paper, we have chosen *soft x-ray* photoemission to study Bi2212, utilizing its (002) Bragg reflection to generate the SW. A photon energy of 930.3 eV was further chosen near an absorption resonance to maximize the SW strength; see the detail in Supplemental Material Fig. S2 [14]. The IMFP for Bi2212 at the excitation energy of ∼930 eV calculated from the TPP-2M formula [5] is ∼1.5 nm. Given that the intensity of collected photoelectrons decays as $\exp(-L/\lambda_{\mathrm{IMFP}})$, where L is the depth, ∼99% of the collected photoelectrons are from the top three unit cells of Bi2212. For the excitation energies of 20–150 eV, ∼99% of the collected photoelectrons are from only the first unit cell of Bi2212. Therefore, the excitation energy of ∼930 eV is relatively sufficient to determine the bulk electronic structure. With the lower energy, it enables higher energy resolution and greater sensitivity to electron momentum than with a higher multi-keV energy. Choosing the soft x-ray of ∼930 eV thus means simultaneously having higher reflectivity, sufficient bulk sensitivity, reasonable energy resolution, and better sensitivity to electron momentum, making it superior to hard x-ray excitation for our SW x-ray photoemission spectroscopy (XPS) study.

II. EXPERIMENTAL AND COMPUTATIONAL DETAILS

The Bi2212 single crystal in this work is optimally doped, and the critical temperature (T_c) determined by superconducting quantum interference device (SQUID) is ∼93K. Details concerning the sample growth and characterization are in Supplemental Material S1 [14]. X-ray reflectivity measurements were performed at beamline 6.3.2 of Advanced Light Source (ALS). The Cr absorption edge (574.1 eV) is used for the energy calibration. ARPES, x-ray absorption spectroscopy (XAS), and SW photoemission (or SW-XPS) measurements were performed at beamline 7.0.2 (MAESTRO) of ALS, and the beamline CASSIOPEE of SOLEIL. The SW-XPS measurement was carried out at ∼77 K, at which the sample was superconducting. Note that the SW-XPS measurement could also be carried out in the normal state, as the temperature and the very small gap at 77 K should have very small impact on the experimental results at this energy resolution.

The reflectivity and SW rocking curve data were analyzed using SW theory based on dynamical x-ray diffraction. The resonant Cu atomic scattering factors were calculated from a Cu L_3 XAS spectrum using Kramers-Kronig relations. The atomic coordinates of Bi2212 with supermodulation were obtained from Ref. [24]. The electronic structures were calculated using the first-principles package QUANTUM ESPRESSO [25] with the generalized gradient approximation (GGA) [26] for the correlation functional, optimized norm-conserving Vanderbilt pseudopotenetials [27] with spin-orbit coupling for core electrons, $10 \times 10 \times 2$ for k-sampling integration and 40 Ry for energy cutoff. Further details are in the Supplemental Material [14].

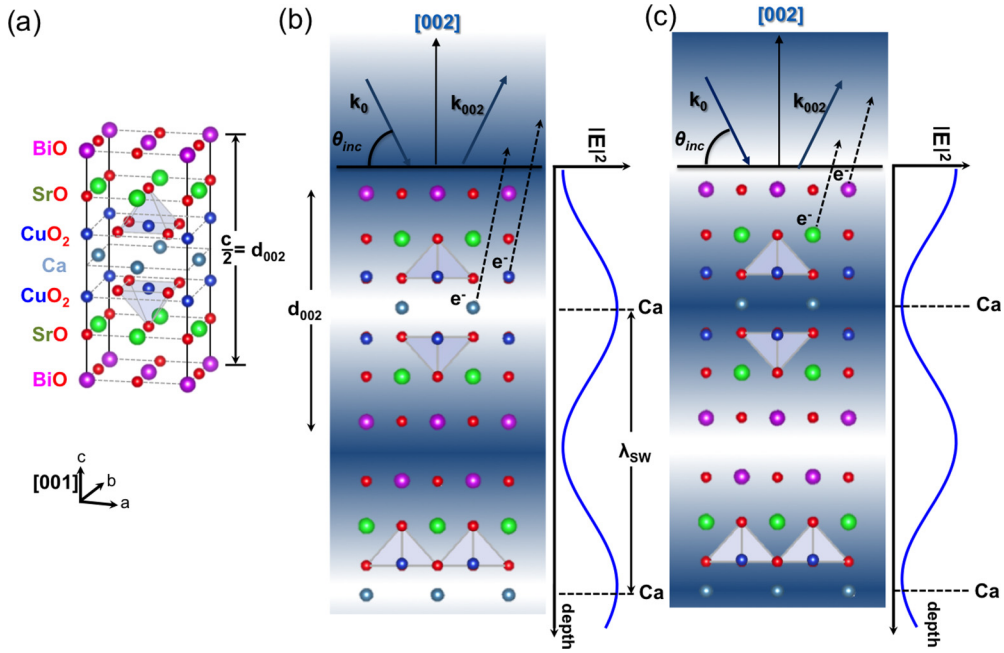

FIG. 1. Spatial relationship between the $Bi_2Sr_2CaCu_2O_{8+\delta}$ (Bi2212) crystal planes and the (002) Bragg-reflection x-ray standing wave (SW). (a) Top half of the unit cell of Bi2212. (b) Schematic of the experimental geometry and the SW generated by the Bi2212 (002) reflection, with wavelength $\lambda_{\mathrm{SW}} = c/2 = d_{002}$. The incident and diffracted waves (associated with wave vectors $\boldsymbol{k_0}$ and $\boldsymbol{k_{002}}$) interfere to produce the SW. The photon energy was 930.3 eV, with a corresponding Bragg angle of about 25.7°. (c) By increasing the incidence angle around the (002) Bragg reflection, the SW can be shifted by $d_{002}/2$. The maximum of the SW electric field intensity can thus be shifted continuously from the Ca plane (b) to the BiO plane (c).

III. RESULTS

A. Standing-wave excited photoemission and rocking curves

A SW with its iso-intensity planes parallel to the diffracting planes is created by the interference between the incident ($\boldsymbol{k}_0$) and diffracted ($\boldsymbol{k}_{002}$) waves [9], as illustrated in Fig. 1. Figure 1(a) shows the Bi2212 crystallographic structure of the top half unit cell, and its cleavage plane primarily occurs in between the BiO layers due to weak van der Waals bonds [1]. The Bi, Sr, Cu, and Ca cations in these layers are well separated along the c-axis direction, making Bi2212 an ideal candidate for applying the SW technique to derive layer-resolved information. From SW theory based on dynamical x-ray diffraction [8,9], the phase difference between the incident and diffracted wave fields changes by π when the incidence angle moves from below to above the Bragg condition, thus scanning the SW by $d_{002}/2$ with respect to the (002) planes, as illustrated in Figs. 1(b) and 1(c). The detailed theoretical SW modeling, including consideration of both x-ray and electron attenuation with depth, is discussed in Supplemental Material S3 [14]. Depending on the locations of the atoms with respect to the scanned SW, the incidence-angle dependence of the core-level photoelectron intensities, which we define as core-level rocking curves (RCs), will show distinct modulations as to both shape and magnitude.

Figures 2 and 3 illustrate the layer-dependent results for core-level intensities using SW excitation. The photoelectron spectra of Ca $2p$, Sr $3d$, Cu $3p$, and Bi $4f_{7/2}$ at an off-Bragg angle (23.2°) are shown in Figs. 2(a)–2(d). Such photoelectron spectra were collected by varying the incidence angle between 24° and 27.5°, yielding the five distinct core-level RCs in Figs. 2(e)–2(i). These RCs are normalized to 1 at off-Bragg positions and have been simulated by SW theory [red curves in Figs. 2(e)–2(i)]. Both members of the spin-orbit split Ca $2p$ spectrum [Fig. 2(a)] exhibit two components, with low-binding-energy (LBE) peaks at 344.6 and 348.1 eV and high-binding-energy (HBE) features at 345.9 and 349.4 eV. These have been observed in previous XPS studies, with varying relative intensities, depending on the sample synthesis procedure [6,28–30]. The RCs of the Ca $2p$(LBE) in Fig. 2(e) and Ca $2p$(HBE) in Fig. 2(f) show different shapes and relative intensity modulations, with LBE exhibiting higher modulation ~8%, as compared to ~5% for HBE. The experimental Ca $2p$(HBE) RC is, within statistical noise, also identical to the Sr $3d$ RC [Fig. 2(g)], including the amplitude of modulation, suggesting that the depths of Ca(HBE) and Sr atoms are essentially identical. By fitting these two experimental Ca $2p$ RCs using Eqs. (S2) and (S3), we are able to derive the values of coherent position (P_{HQ}), which determines the shape of

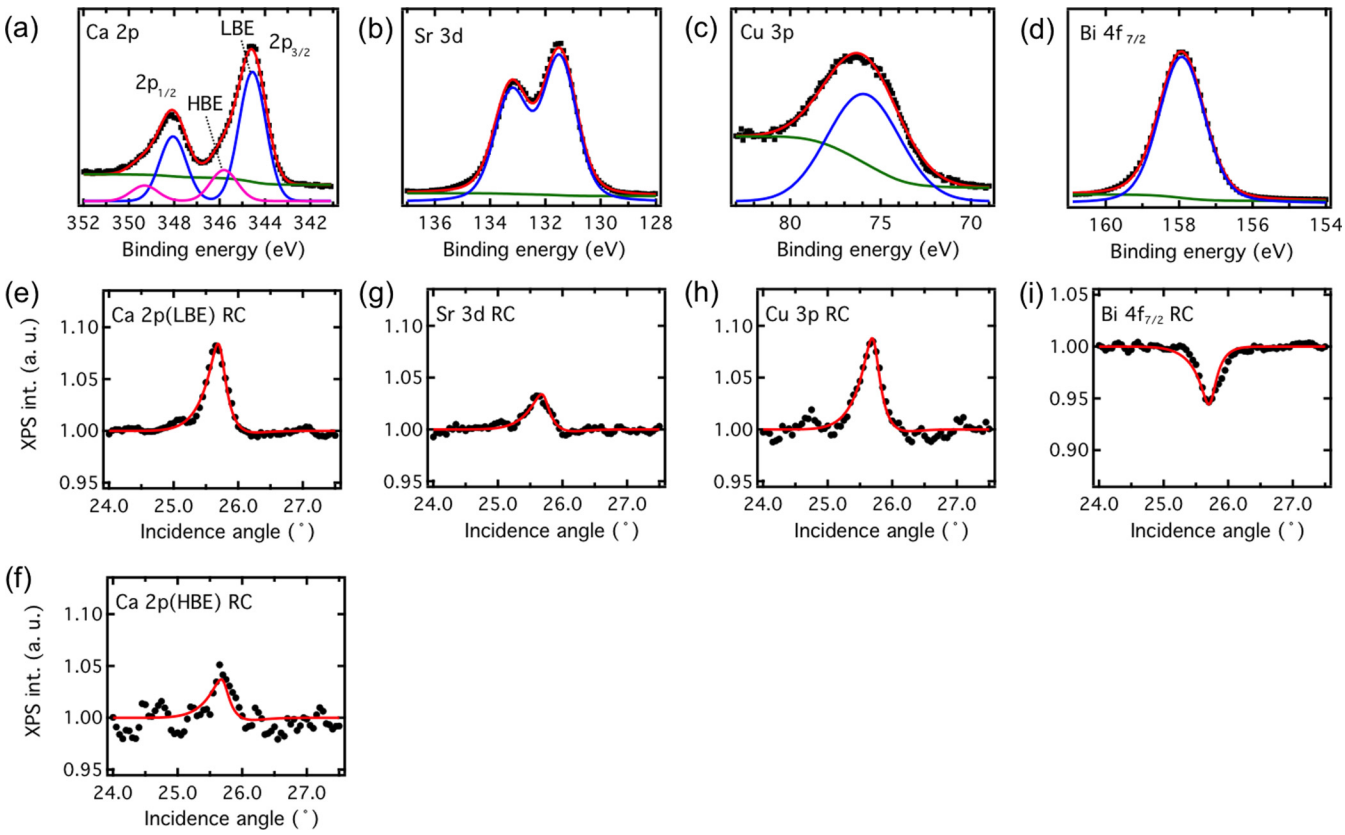

FIG. 2. Bragg-reflection standing-wave x-ray photoemission from the cations of Bi2212 at $h\nu = 930.3$ eV. Core-level spectra of (a) Ca $2p$, (b) Sr $3d$, (c) Cu $3p$, and (d) Bi $4f_{7/2}$ at an off-Bragg incidence angle. The core-level peak intensities are derived by fitting with a Voigt line shape (in blue and magenta) and a Shirley background (in green). The corresponding experimental rocking curves (RCs) of core-level intensities are also plotted in (e)–(i) (black dots) and compared with SW theory (red curves). In (a) Ca $2p$ is found to have high-binding-energy (HBE) and low-binding-energy (LBE) components, which shows different RC behavior as to shape and fractional modulation. The RCs of Ca $2p$ HBE [in (f)] and Sr $3d$ [in (g)] are found to be identical within experimental error, indicating that Ca atoms occupy the Sr sites in the SrO layer.

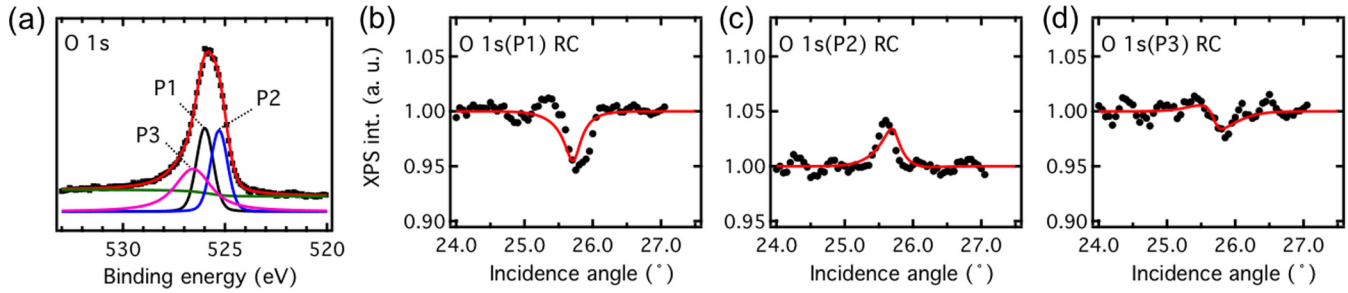

FIG. 3. Bragg-reflection standing-wave x-ray photoemission from the oxygen atoms of Bi2212. (a) Core-level spectrum of O 1*s* at an off-Bragg incidence angle. The O1*s* spectrum is known to contain three components (P1, P2, and P3). The RCs of (b) P1, (c) P2, and (d) P3 exhibit distinct shape and intensity modulations; these can be assigned through SW analysis (red curves) to different layers. The O(P1) atoms are located in the BiO layer. The O(P2) atoms are in the CuO_2 layer with a vertical offset of $\sim 0.9 \pm 0.5$ Å to the Cu atoms. The O(P3) atoms are in the SrO layer with a vertical offset of $\sim 1.5 \pm 0.5$ Å.

RCs and provides the averaged locations of Ca(HBE) and Ca(LBE) atoms. Detailed discussions regarding the parameters on fitting the experimental RCs and a summary Table S1 can be found in Supplemental Material S3 [14]. Thus, we can unambiguously conclude that the Ca(LBE) atoms are located in the Ca layer, while the Ca(HBE) atoms are located in the SrO layer, implying that a significant fraction of Ca atoms occupy the Sr sites during synthesis.

A more quantitative analysis was made by considering the peak intensity ratio, $I(\text{HBE})/[I(\text{HBE}) + I(\text{LBE})]$ away from the Bragg reflection, which is $\sim$0.2 with respect to the ideal amount of Ca; this indicates that an excess of $\sim$10% Ca is intermixing with each of the two adjacent SrO layers. Previous work on the degree of Sr-Ca intermixing is controversial [6,28–30], with some studies suggesting pronounced Sr-Ca intermixing in both Ca and SrO layers [28] and some claiming low intermixing but with strong dependence on sample preparation [29,30]. For our sample, both the observation of only one component in the Sr 3*d* spectrum and its RC show that the Sr atoms are located in a single layer without intermixing. Note that although the chemical composition of Bi2212 here is referred to $Bi_2Sr_2CaCu_2O_{8+\delta}$, the actual thermodynamically stable composition can be deficient in Sr and Ca while being Bi rich. For example, Mitzi *et al.* found that the stable composition, by normalizing Cu to be 2, is $Bi_{2.03}Sr_{1.87}Ca_{0.85}Cu_2O_{8+\delta}$ and the precise numbers in fact vary from sample to sample [31]. In our work, from two successful SW-XPS measurements on cleaved Bi2212 samples, the quantity of intermixing shows no noticeable difference; however, these two samples come from the same large crystal and should exhibit similar stoichiometry. The quantity of intermixing can vary with different crystal preparations [31], a possible subject of future study with standing-wave excitation.

The Cu 3*p* and Bi 4*f* spectra in Figs. 2(c) and 2(d) also show single components, although Cu 3*p* is broad, as seen previously [7], and their very different RCs [Figs. 2(h)–2(i)] demonstrate that the Cu and Bi atoms are uniquely located in their own layers. Note that the *shape* of the Sr 3*d* and Cu 3*p* RCs are close, which is not surprising in view of the location of Sr atoms on either side of the Cu atoms, but the Cu 3*p* RC shows a stronger intensity modulation due to the lack of the SW phase averaging over the two Sr layers in the half unit cell. All of these conclusions are supported by the excellent agreement between experiment and SW modeling in Figs. 2(e)–2(i).

We now consider the O 1*s* spectrum in Fig. 3(a), which is thought from prior XPS work to exhibit three components contributed from the different atomic layers [32,33]. Through modeling the O1*s* RCs with SW theory, the locations of these components were determined. The O 1*s*(P1) RC [Fig. 3(b)] shows that these oxygen atoms are located in the BiO layer. The O 1*s*(P2) RC in Fig. 3(c) has a similar shape but weaker intensity modulation compared to the Cu 3*p* RC, suggesting that, in the first CuO layer, the O(P2) atoms are $\sim 0.9 \pm 0.5$ Å higher than Cu atoms. O 1*s*(P3) RC [Fig. 3(d)] is slightly out of phase with respect to the Sr 3*d* RC, suggesting that, in the first SrO layer, the P3 oxygen atoms are $\sim 1.5 \pm 0.5$ Å higher relative to Sr atoms. These SW-determined locations of the oxygen atoms are in good agreement with prior transmission electron microscopy and x-ray diffraction results [24,34]. Looking ahead, future SW photoemission studies of Bi2212 or other cuprates, with higher reflectivities and better statistics, and with various oxygen dopant levels, should be able to determine the O stoichiometries in each layer and thus answer the question of where the additional oxygen dopant atoms reside.

In addition, these SW results provide unique insight into the chemical/electronic disorder along the *c* axis in cuprates. In a broader perspective, several cuprate studies have demonstrated the interesting out-of-plane electronic properties. For example, YBCO exhibits a three-dimensional charge ordering at high magnetic fields [35,36]. The *c*-axis resistivity has been used to reveal information on the pseudogap phase [37] and magnetotransport [38] as well as soft x-ray ARPES [39] about the Fermi surface warping. Coming back to our work, the chemical disorder along the *c* axis might prevent three-dimensional charge order in Bi2212 and also give rise to a larger scattering in *c*-axis resistivity experiments. Future experiments exploring these chemical/electronic effects in more detail should be very interesting.

B. Atomic-layer-resolved electronic structure

In order to resolve the individual atomic layer contributions to the Bi2212 valence band (VB), we measured the VB RCs, which is an intensity map $I_{\text{VB}}(E_b, \theta_{\text{inc}})$, with binding energy ($E_b$) and incidence angle ($\theta_{\text{inc}}$), over an angle scan. The VB

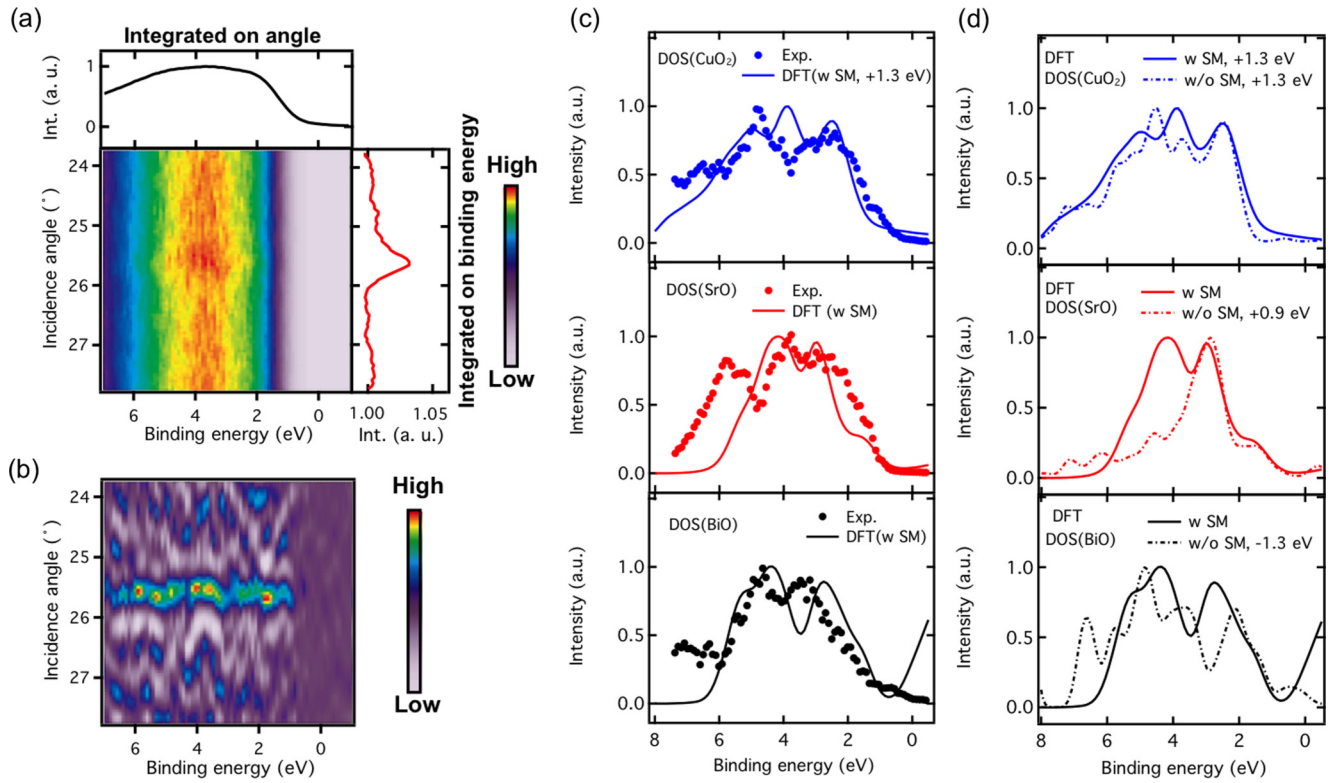

FIG. 4. Standing-wave valence-band (VB) spectra and atomic-layer-resolved, cross-section-weighted densities of states (DOSs) together with DFT calculations. (a) VB intensity map for different incidence angles, with the color scale corresponding to the photoemission intensity, and top and right curves representing integrals over incidence angle and binding energy, respectively. (b) As (a), but for the second-derivative of intensity. The Bragg-reflection maximum is at ∼25.7°, and the VB intensities exhibit modulations that are associated with the variable layer-specific contributions along the binding energy axis; this is particularly evident in the second derivative plot. (c) The layer-projected DOSs of CuO_2 (blue dots), SrO (red dots), and BiO (black dots) and the corresponding layer-projected DOSs from DFT calculations including supermodulation in the crystal structure (solid line). (d) The comparison of DFT results with supermodulation (w SM) structures (solid line) and without supermodulation (w/o SM) structures are shown (dot-dashed line). Various energy shifts have been applied to theory in (c) and (d) to yield the best agreement with experiment; with supermodulation, only the CuO_2 DOS requires a shift.

RCs can be written as a superposition of the experimentally layer-projected and cross-section-weighted DOSs in the different layers, $D_i(E_b) \approx \sum_{i,Qnl} \frac{d\sigma_{Qnl}}{d\Omega} \rho_{Qnl}(E_b)$, multiplied by layer-dependent normalized core-level RCs $\bar{I}_{Qn'l'}(\theta_{\rm inc})$, as discussed previously [11,12,13,40–43], see further details in Supplemental Material S4 [14]. That is,

$$I_{\rm VB}(E_b, \theta_{\rm inc}) = \sum_{Qnl} D_{Qnl}(E_b) \bar{I}_{Qn'l'}(\theta_{\rm inc}). \quad (1)$$

Here $Qn\ell$ denotes a valence level $n\ell$ in the atom Q, and $Qn'\ell'$ a core level in the same atom, and $\bar{I}_{Qn'l'}(\theta_{\rm inc})$ is the RC for $Qn'\ell'$, normalized to unity away from the Bragg reflection. For our case, $Qn'\ell' =$ Cu $3p$, Sr $3d$, and Bi $4f_{7/2}$.

The main contributions from the atomic orbitals in the layer-projected DOSs based on strength of hybridization and photoelectric cross sections at our excitation energy are Cu $3d$ in CuO_2, Sr $4p$ in SrO, and Bi $5d$ in BiO (see Supplemental Material S5 [14]). The Ca $4s$ orbitals in the Ca layer are negligible, as discussed in prior work using density functional theory (DFT) calculations in the local-density approximation (LDA) [44,45]. In both the raw data for $I_{\rm VB}(E_b, \theta_{\rm inc})$ of Fig. 4(a) and in a more pronounced way in its second derivative along the axis of incidence angle in Fig. 4(b), there are intensity modulations with BE associated with the different layer contributions to the intensity; these are particularly clear along the Bragg angle at ∼25.7°. The VB RCs for each BE have been fitted to a linear combination of these three core-level RCs by a least-squares method, and the resultant fitting coefficients correspond to the layer-resolved cross-section-weighted DOSs $D_i(E_b)$.

Figure 4(c) shows these experimental layer-projected cross-section-weighted DOSs (dots) in comparison to DFT calculations (curves) incorporating the supermodulation displacements known to exist in Bi2212 [14], in particular with a twofold enlargement of the unit cell size in the x-y plane (see Supplemental Material S6 [14]). The $D_{\rm CuO_2}(E_b)$ and $D_{\rm BiO}(E_b)$ show good agreement with the DFT results including supermodulation. The $D_{\rm SrO}(E_b)$ is however considerably broader than the DFT results. One obvious source of uncertainty and broadening has been mentioned before: the Sr $3d$ RC has a similar shape compared to the Cu $3p$ RC, meaning that the deconvolution procedure will inherently mix some intensity from CuO_2. Beyond this, the broadening of $D_{\rm SrO}(E_b)$ is certainly associated with the significant Ca-Sr intermixing, causing more disorder and scattering. Further electronic structure calculations, e.g., within the coherent potential approximation, would help to test this hypothesis.

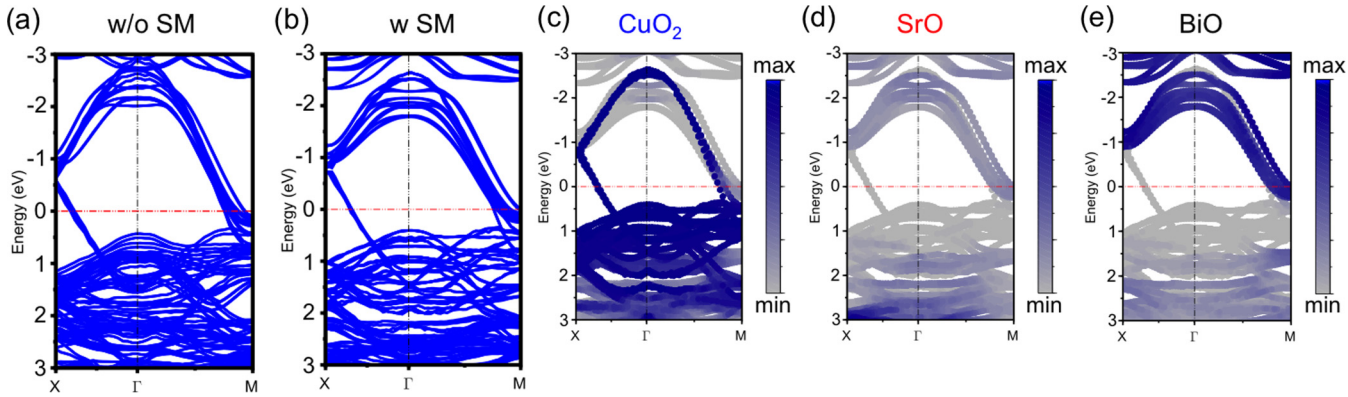

FIG. 5. Band structure in the high-symmetry directions near the E_F. Full band structure for Bi2212 without (a) and with (b) supermodulation effect in the crystal structure. The layer-projected (c) CuO_2, (d) SrO, and (e) BiO band structures of (b) (with supermodulation). The blue-to-grey color scale indicates strong-to-weak contribution from a given layer. Note that no energy shift is applied to theory here.

IV. DISCUSSION

To assist in understanding the influence of the supermodulated atomic displacements on the electronic structure, the layer-projected DOSs with and without supermodulation are plotted together in Fig. 4(d). The introduction of supermodulation makes no significant difference in the CuO_2 DOS, but for both cases, a shift to higher BE by 1.3 eV is necessary to reach agreement with the experimental $D_{CuO_2}(E_b)$. For the DOSs of the SrO and BiO layers, no BE shift is needed for the supermodulation results, whereas without supermodulation, one needs to shift the curves to higher BE by 0.9 eV and to lower BE by 1.3 eV to best match experiment, respectively. Adding supermodulation for the SrO DOS further produces an additional peak at ∼5 eV that much better matches the experimental $D_{SrO}(E_b)$. For the BiO plane, the disappearance of a peak at ∼6.5 eV in the theoretical DOS with supermodulation structure is again in better agreement with the experimental $D_{BiO}(E_b)$. In summary, taking supermodulation into consideration leads to a change of the SrO and BiO DOSs, improving the agreement with the layer-projected DOSs. This indicates the strong influence of the supermodulation structure on the electronic structure of Bi2212.

We have noted that an energy shift of the theoretical CuO_2 DOS to 1.3 eV higher BE has been necessary to match the $D_{CuO_2}(E_b)$. Such shifts of the VB energies in photoemission relative to LDA calculations have been widely reported in the cuprates (e.g., LSCO [46], YBCO [46], and Bi2212 [47]). In undoped cuprates the Coulomb interaction between the Cu $3d$ electrons in cuprates, which is not treated fully in simple DFT calculations, can lead to the opening of a Mott-Hubbard gap, with a bound-state energy shift to higher BE and a lower DOS in the vicinity of the Fermi energy (E_F) [46,47]. These features in the cuprate VBs are spectroscopic evidence of strong correlation effects, and more detailed discussions can be found elsewhere [48]. In metallic cuprates, where the Cu $3d$ states hybridized with O $2p$ dates mostly lie 2–6 eV below the Fermi level, the main effect relevant to the current data is an increase in binding energy. The $D_{CuO_2}(E_b)$ thus shows that the energy shift that can be attributed to this electron correlation effect is 1.3 eV.

In order to visualize in more detail the layered-resolved electronic structure of Bi2212, the band structures near the E_F region are shown in Fig. 5. The full band structure without supermodulation is shown in Fig. 5(a), and in Fig. 5(b) with supermodulation. The band structure in Fig. 5(a) is in good agreement with prior work [44,45]. By comparing these two figures, one clearly sees a splitting of the bands (at ~ -2 eV and at 0.5–2 eV BE) that results from including supermodulation. For the more realistic band structure with supermodulation we now show the layer-projected band structures in Figs. 5(c)–5(e) in a blue-gray scale to indicate relative amplitude. From these results alone, one would conclude that, around the M point, the Fermi surface of Bi2212 is governed by the CuO_2 bands, but that there is also a strong contribution from the BiO bands. Although our DFT results show the existence of BiO bands near the M point [Fig. 5(e)] and some BiO state intensity extending below E_F [Fig. 4(c)], our experimental results in the same figure lack that spectral feature, in agreement with previous photoemission studies [1,6]. For example, to resolve this disagreement between the DFT results and photoemission, Lin *et al.* [49] proposed that, with increasing oxygen doping in the BiO layer, the BiO band shifts above E_F at the M point, which also is consistent with a scanning tunneling microscopic and spectroscopic study [50]. The excess oxygen atoms are believed to be responsible for the δ in the common designation $Bi_2Sr_2CaCu_2O_{8+\delta}$.

V. CONCLUSIONS

In summary, we have carried out soft x-ray SW photoemission study of Bi2212 and derived the depth distribution of atoms within one unit cell, in particular, a 10% Ca-Sr intermixing and the three types of oxygen atoms bonding to different cations. In addition, we have successfully decomposed the electronic structure of Bi2212 into atomic-layer-specific, matrix-element-weighted DOSs. These atomic-layer-resolved DOSs show good agreement with DFT calculations in most respects, provided we incorporate the known supermodulation structure in Bi2212. Our results for the layer-resolved electronic structure are found to be strongly influenced by the supermodulation, Ca-Sr intermixing, and the Cu $3d$-$3d$ Coulomb interaction, further clarifying the complexity of this prototypical cuprate. Future measurements of this type for other cuprates should yield equally unique information, such as providing insights on how the T_c increases while

stacking more CuO_2 layers from bi-layered Bi2212 to tri-layered $Bi_2Sr_2Ca_2Cu_3O_{10+\delta}$ (Bi2223). Bragg-reflection SW photoemission is thus very promising for the study of quasi-2D materials with large-c lattice parameters.

ACKNOWLEDGMENTS

The authors thank Jonathan Denlinger and Simon Moser for their comments concerning Bi2212 sample preparation. We thank synchrotron SOLEIL (via Proposal No. 20161205) for access to Beamline CASSIOPEE that contributed to the results presented here. This work was supported by the US Department of Energy (DOE) under Contract No. DE-AC02-05CH11231 (Advanced Light Source), and by DOE Contract No. DE-SC0014697 through the University of California Davis (C.-T.K, S.-C.L., and C.S.F.). S.-T. Pi was supported by DOE Grant No. DE-NA0002908. C.S.F. has also been supported by the Director, Office of Science, Office of Basic Energy Sciences (BSE), Materials Sciences and Engineering (MSE) Division, of the US Department of Energy under Contract No. DE-AC02-05CH11231, through the Laboratory Directed Research and Development Program of Lawrence Berkeley National Laboratory, through a DOE BES MSE grant at the University of California Davis from the X-Ray Scattering Program under Contract No. DE-SC0014697, through the APTCOM Project, "Laboratoire d'Excellence Physics Atom Light Matter" (LabEx PALM) overseen by the French National Research Agency (ANR) as part of the "Investissements d'Avenir" program, and from the Jülich Research Center, Peter Grünberg Institute, PGI-6. Support for W.E.P. was provided by DOE Grant No. DE-FG02-04ER46111. This research used resources of the National Energy Research Scientific Computing Center (NERSC), a DOE Office of Science User Facility supported by the Office of Science of the U.S. Department of Energy under Contract No. DE-AC02-05CH11231.

[1] A. Damascelli, Z. Hussain, and Z.-X. Shen, Rev. Mod. Phys. **75**, 473 (2003).
[2] Ø. Fisher, M. Kugler, I. Maggio-Aprile, C. Berthod, and C. Renner, Rev. Mod. Phys. **79**, 353 (2007).
[3] F. J. Himpsel, Adv. Phys. **32**, 1 (1983).
[4] M. Z. Hasan and C. L. Kane, Rev. Mod. Phys. **82**, 3045 (2010).
[5] S. Tanuma, C. J. Powell, and D. R. Penn, Surf. Interface Anal. **43**, 689 (2011).
[6] P. A. P. Lindberg, Z.-X. Shen, W. E. Spicer, and I. Lindau, Surf. Sci. Rep. **11**, 1 (1990).
[7] M. Qvarford, J. F. van Acker, J. N. Andersen, R. Nyholm, I. Lindau, G. Chiaia, E. Lundgren, S. Söderholm, U. O. Karlsson, S. A. Flodström, and L. Leonyuk, Phys. Rev. B **51**, 410 (1995).
[8] B. W. Batterman and H. Cole, Rev. Mod. Phys. **36**, 681 (1964).
[9] I. A. Vartanyants and M. V. Kovalchuk, Rep. Prog. Phys. **64**, 1009 (2001).
[10] J. C. Woicik, E. J. Nelson, and P. Pianetta, Phys. Rev. Lett. **84**, 773 (2000).
[11] J. C. Woicik, E. J. Nelson, D. Heskett, J. Warner, L. E. Berman, B. A. Karlin, I. A. Vartanyants, M. Z. Hasan, T. Kendelewicz, Z. X. Shen, and P. Pianetta, Phys. Rev. B **63**, 041403(R) (2001).
[12] S. Thiess, T.-L. Lee, F. Bottin, and J. Zegenhagen, Solid State Commun. **150**, 553 (2010).
[13] S. Thiess, T.-L. Lee, C. Aruta, C. T. Lin, F. Venturini, N. B. Brookes, B. C. C. Cowie, and J. Zegenhagen, Phys. Rev. B **92**, 075117 (2015).
[14] See Supplemental Material at http://link.aps.org/supplemental/10.1103/PhysRevB.98.155133 for details on the sample preparation and characterization, the resonant effect, the reflectivity and SW modeling, the photoelectric cross-section-weighted DOSs, and the atomic coordinates for DFT calculations, which includes Refs. [1,8,9,11,15–24,34,40–42].
[15] P. Aebi, J. Osterwalder, P. Schwaller, L. Schlapbach, M. Shimoda, T. Mochiku, and K. Kadowaki, Phys. Rev. Lett. **72**, 2757 (1994).
[16] A. X. Gray, C. Papp, B. Balke, S.-H. Yang, M. Huijben, E. Rotenberg, A. Bostwick, S. Ueda, Y. Yamashita, K. Kobayashi, E. M. Gullikson, J. B. Kortright, F. M. F. de Groot, G. Rijnders, D. H. A. Blank, R. Ramesh, and C. S. Fadley, Phys. Rev. B **82**, 205116 (2010).
[17] A. Kazimirov, T. Haage, L. Ortega, A. Stierle, F. Comin, and J. Zegenhagen, Solid State Commun. **104**, 347 (1997).
[18] A. Kazimirov, N. Faleev, H. Temkin, M. J. Bedzyk, V. Dmitriev, and Y. Melnik, J. Appl. Phys. **89**, 6092 (2001).
[19] Y. He, S. Graser, P. Hirschfeld, and H.-P. Cheng, Phys. Rev. B **77**, 220507 (2008).
[20] J. W. Cooper, Phys. Rev. A **47**, 1841 (1993).
[21] J. J. Yeh and I. Lindau, At. Data Nucl. Data Tables **32**, 1 (1985).
[22] J. K. Liang, S. S. Xie, G. C. Che, J. Q. Huang, Y. L. Zhang, and Z. X. Zhao, Mod. Phys. Lett. B **2**, 483 (1988).
[23] A. A. Levin, Y. I. Smolin, and Y. F. Shepelev, J. Phys.: Condens. Matter **6**, 3539 (1994).
[24] M. Hervieu, C. Michel, B. Domenges, Y. Laligant, A. Lebail, G. Ferey, and B. Raveau, Mod. Phys. Lett. B **2**, 491 (1988).
[25] P. Giannozzi, S. Baroni, N. Bonini, M. Calandra, R. Car, C. Cavazzoni, D. Ceresoli, G. L. Chiarotti, M. Cococcioni, I. Dabo, A. D. Corso, S. de Gironcoli, S. Fabris, G. Fratesi, R. Gebauer, U. Gerstmann, C. Gougoussis, A. Kokalj, M. Lazzeri, L. Martin-Samos, N. Marzari, F. Mauri, R. Mazzarello, S. Paolini, A. Pasquarello, L. Paulatto, C. Sbraccia, S. Scandolo, G. Sclauzero, A. P. Seitsonen, A. Smogunov, P. Umari, and R. M. Wentzcovitch, J. Phys.: Condens. Matter **21**, 395502 (2009).
[26] J. P. Perdew, K. Burke, and M. Ernzerhof, Phys. Rev. Lett. **77**, 3865 (1996).
[27] D. R. Hamann, Phys. Rev. B **88**, 085117 (2013).
[28] S. Kohiki, T. Wada, S. Kawashima, H. Takagi, S. Uchida, and S. Tanaka, Phys. Rev. B **38**, 7051 (1988).
[29] F. U. Hillebrecht, J. Fraxedas, L. Ley, H. J. Trodahl, J. Zaanen, W. Braun, M. Mast, H. Petersen, M. Schaible, L. C. Bourne, P. Pinsukanjana, and A. Zettl, Phys. Rev. B **39**, 236 (1989).
[30] H. M. Meyer, III, D. M. Hill, J. H. Weaver, D. L. Nelson, and C. F. Gallo, Phys. Rev. B **38**, 7144(R) (1988).
[31] D. B. Mitzi, L. W. Lombardo, A. Kapitulnik, S. S. Laderman, and R. D. Jacowitz, Phys. Rev. B **41**, 6564 (1990).

[32] F. Parmigiani, Z. X. Shen, D. B. Mitzi, I. Lindau, W. E. Spicer, and A. Kapitulnik, Phys. Rev. B **43**, 3085 (1991).
[33] M. Qvarford, S. Söderholm, G. Chiaia, R. Nyholm, J. N. Andersen, I. Lindau, U. O. Karlsson, L. Leonyuk, A. Nilsson, and N. Martensson, Phys. Rev. B **53**, R14753 (1996).
[34] S. A. Sunshine, T. Siegrist, L. F. Schneemeyer, D. W. Murphy, R. J. Cava, B. Batlogg, R. B. van Dover, R. M. Fleming, S. H. Glarum, S. Nakahara, R. Farrow, J. J. Krajewski, S. M. Zahurak, J. V. Waszczak, J. H. Marshall, P. Marsh, L. W. Rupp, Jr., and W. F. Peck, Phys. Rev. B **38**, 893 (1988).
[35] S. Gerber, H. Jang, H. Nojiri, S. Matsuzawa, H. Yasumura, D. A. Bonn, R. Liang, W. N. Hardy, Z. Islam, A. Mehta, S. Song, M. Sikorski, D. Stefanescu, Y. Feng, S. A. Kivelson, T. P. Devereaux, Z.-X. Shen, C.-C. Kao, W.-S. Lee, D. Zhu, and J.-S. Lee, Science **350**, 949 (2015).
[36] J. Chang, E. Blackburn, O. Ivashko, A. T. Holmes, N. B. Christensen, M. Hücker, Ruixing Liang, D. A. Bonn, W. N. Hardy, U. Rütt, M. v. Zimmermann, E. M. Forgan, and S. M. Hayden, Nat. Commun. **7**, 11494 (2016).
[37] G. Sordi, P. Sémon, K. Haule, and A.-M. S. Tremblay, Phys. Rev. B **87**, 041101(R) (2013).
[38] N. E. Hussey, M. Abdel-Jaward, A. Carrington, A. P. Mackenzie, and L. Balicas, Nature (London) **425**, 814 (2003).
[39] M. Horio, K. Hauser, Y. Sassa, Z. Mingazheva, D. Sutter, K. Kramer, A. Cook, E. Nocerino, O. K. Forslund, O. Tjernberg, M. Kobayashi, A. Chikina, N. B. M. Schröter, J. A. Krieger, T. Schmitt, V. N. Strocov, S. Pyon, T. Takayama, H. Takagi, O. J. Lipscombe, S. M. Hayden, M. Ishikado, H. Eisaki, T. Neupert, M. Månsson, C. E. Matt, and J. Chang, Phys. Rev. Lett. **121**, 077004 (2018).
[40] A. M. Kaiser, A. X. Gray, G. Conti, J. Son, A. Greer, A. Perona, A. Rattanachata, A. Y. Saw, A. Bostwick, S. Yang, S.-H. Yang, E. M. Gullikson, J. B. Kortright, S. Stemmer, and C. S. Fadley, Phys. Rev. Lett. **107**, 116402 (2011).
[41] U. Gelius, in *Electron Spectroscopy*, edited by D. A. Shirley (North Holland, Amsterdam, 1971), p. 311.
[42] C. Solterbeck, W. Schattke, J.-W. Zahlmann-Nowitzki, K.-U. Gawlik, L. Kipp, M. Skibowski, C. S. Fadley, and M. A. Van Hove, Phys. Rev. Lett. **79**, 4681 (1997).
[43] A. X. Gray, J. Minár, S. Ueda, P. R. Stone, Y. Yamashita, J. Fujii, J. Braun, L. Plucinski, C. M. Schneider, G. Panaccione, H. Ebert, O. D. Dubon, K. Kobayashi, and C. S. Fadley, Nat. Mater. **11**, 957 (2012).
[44] H. Krakauer and W. E. Pickett, Phys. Rev. Lett. **60**, 1665 (1988).
[45] L. F. Mattheiss and D. R. Hamann, Phys. Rev. B **38**, 5012 (1988).
[46] A. Fujimori, E. Takayama-Muromachi, Y. Uchida, and B. Okai, Phys. Rev. B **35**, 8814 (1987).
[47] Z.-X. Shen, P. A. P. Lindberg, I. Lindau, W. E. Spicer, C. B. Eom, and T. H. Geballe, Phys. Rev. B **38**, 7152 (1988).
[48] Z.-X. Shen and D. S. Dessau, Phys. Rep. **253**, 1 (1995).
[49] H. Lin, S. Sahrakorpi, R. S. Markiewicz, and A. Bansil, Phys. Rev. Lett. **96**, 097001 (2006).
[50] K. McElroy, J. Lee, J. A. Slezak, D.-H. Lee, H. Eisaki, S. Uchida, and J. C. Davis, Science **309**, 1048 (2005).